TECHNICAL ARTICLE

Temperature-dependent structural behaviour of samarium cobalt oxide

Matthew R. Rowles,[1,a] Cheng-Cheng Wang,[1] Kongfa Chen,[1] Na Li,[1,2] Shuai He,[1] and San-Ping Jiang[1]
[1]*Fuels and Energy Technology Institute, Curtin University, GPO Box U1987, Perth WA 6185, Australia*
[2]*College of Science, Heilongjiang University of Science and Technology, Harbin 150022, China*

(Received 1 March 2017; accepted 12 July 2017)

The crystal structure and thermal expansion of the perovskite samarium cobalt oxide ($SmCoO_3$) have been determined over the temperature range 295–1245 K by Rietveld analysis of X-ray powder diffraction data. Polycrystalline samples were prepared by a sol–gel synthesis route followed by high-temperature calcination in air. $SmCoO_3$ is orthorhombic (*Pnma*) at all temperatures and is isostructural with $GdFeO_3$. The structure was refined as a distortion mode of a parent $Pm\bar{3}m$ structure. The thermal expansion was found to be non-linear and anisotropic, with maximum average linear thermal expansion coefficients of $34.0(3) \times 10^{-6}$, $24.05(17) \times 10^{-6}$, and $24.10(18) \times 10^{-6}$ K^{-1} along the *a*-, *b*-, and *c*-axes, respectively, between 814 and 875 K. © *2017 International Centre for Diffraction Data.*
[doi:10.1017/S0885715617000872]

Key words: structure determination, thermal expansion, solid-oxide fuel cell

I. INTRODUCTION

Cobaltite perovskite oxides such as $(La,Sr)CoO_{3-\delta}$ (LSC), $(Sm,Sr)CoO_{3-\delta}$ (SSC), and $(Ba,Sr)(Co,Fe)O_{3-\delta}$ (BSCF) are mixed ionic/electronic conductors with high electrocatalytic activity to promote oxygen reduction required for their use as cathodes in solid-oxide fuel cells (Sun *et al.*, 2009). Compared with LSC, SSC, with a smaller cation in the A site (Sm vs. La), has been demonstrated to show much better oxygen surface exchange kinetics (Fukunaga *et al.*, 2000). Therefore, SSC has been extensively investigated as a promising cathode material for intermediate-temperature solid-oxide fuel cells (Tu *et al.*, 1997; Ishihara *et al.*, 1998; Xia *et al.*, 2002; Yang *et al.*, 2008; Dong *et al.*, 2012).

The room-temperature structure of the SSC end-member, $SmCoO_3$, has been studied previously in the context of solid-solution series with Ni (Pérez-Cacho *et al.*, 2000), Fe (Kharko *et al.*, 2014), and Sr (Tu *et al.*, 1997), which, in all cases, was reported as the orthorhombic *Pbnm* space-group [standard setting *Pnma*, no. 62 (Hahn, 1995)]. Tu *et al.* (1997) do report the rate of $SmCoO_3$ thermal expansion up to 1000 °C; however, this was measured on bulk, polycrystalline specimens, and reveals no information about any thermal expansion dependence on crystallographic parameters.

The aim of our research programme is to investigate the atomic structure, thermal expansion behaviour, and electrochemical properties of various perovskites in order to correlate their structural parameters and behaviour as a solid-oxide fuel cell cathode. This work reports the temperature-dependent structure of $SmCoO_3$ from room temperature to 1245 K.

II. EXPERIMENTAL

A. Sample preparation

$SmCoO_{3-\delta}$ powder was synthesised by the combined citrate and ethylenediaminetetraacetic acid (EDTA) complexing method (Wang *et al.*, 2009; Shao *et al.*, 2012; Chen *et al.*, 2016). The raw chemicals were $Sm(NO_3)_3 \cdot 6H_2O$ (99%, Sigma-Aldrich), $Co(NO_3)_2 \cdot 6H_2O$ (98.0–102.0%, Alfa-Aesar), citric acid (99.5%, Chem Supply), EDTA (99%, Acros Organics), and ammonia (28%, Ajax Finechem). The molar ratio of metal ions/citric acid/EDTA was 1:1.5:1. The resultant powder was calcined at 900 °C in air for 2 h.

B. *In situ* synchrotron X-ray powder diffraction

High-resolution X-ray powder diffraction patterns were collected using the Powder Diffraction beamline (Wallwork *et al.*, 2007) at the Australian Synchrotron. A monochromatic X-ray beam with an energy of 15.5108 keV [determined from LaB_6 (NIST SRM 660b)] was used in order to keep away from the Sm L absorption edge to avoid spurious detector effects arising from specimen fluorescence. Data were collected over the angular range 3–83°2θ using an array of Mythen position sensitive detector modules (Schmitt *et al.*, 2003). To eliminate the gaps between the individual Mythen modules, the diffraction patterns were acquired in pairs with a goniometer rotation of 0.5°2θ between each pattern, and merged using the program CONVAS2 (Rowles, 2012). The $SmCoO_3$ powder was loaded in a 0.5 mm quartz capillary and mounted in Debye–Scherrer geometry. The capillary was continuously rotated about its long axis at ~1 Hz in order to provide even heating, improve particle statistics, and ensure accurate relative peak intensities.

The specimen was heated using a hot-air blower at a constant rate of 8 K min^{-1} from room temperature up to 1245 K before cooling as rapidly as possible. The temperature was controlled by a thermocouple placed between the nozzle of the hot-air blower and the capillary. The specimen temperature

[a]Author to whom correspondence should be addressed. Electronic mail: matthew.rowles@curtin.edu.au

was calibrated (Stinton and Evans, 2007) using the known thermal expansion coefficients (TECs) of corundum (Taylor, 1984) applied to NIST SRM 676a. *In situ* diffraction patterns were collected for 45 s in each goniometer position, with approximately 13 s between each diffraction pattern for goniometer movement, for the duration of the experiment.

III. RESULTS AND DISCUSSION

Select diffraction patterns over the entire temperature range were indexed by the SVDIndex algorithm (Coelho, 2003) in TOPAS (Bruker AXS, 2014) and were all found to be consistent with the orthorhombic space-group *Pnma*, as has been found in previous room-temperature studies (Tu *et al.*, 1997; Pérez-Cacho *et al.*, 2000; Kharko *et al.*, 2014). There were several unidentified minor impurity peaks present, but they were able to be discounted, as their thermal expansion behaviour was markedly different to that of the main perovskite phase.

All diffraction data were analysed by the Rietveld method (Rietveld, 1969) as implemented in TOPAS. Refined parameters included background coefficients, specimen displacement (Scarlett *et al.*, 2011), lattice parameters, profile coefficients, atomic position coordinates, and isotropic atomic displacement parameters. The zero offset was constrained to be the same over all patterns. The effect of specimen absorption and capillary geometry on peak intensities and profiles was modelled using a capillary aberration function based on the work of Sabine *et al.* (1998). The temperature calibration data were parametrically refined (Stinton and Evans, 2007) to give the actual specimen temperature, which was then used unchanged. The isotropic displacement parameters of all atoms were found to vary quadratically with temperature, and were so constrained to this in the refinement, with only the coefficients of the quadratic being refined. Refinement of anisotropic displacement parameters was attempted, but was not found to be supported by the data.

The atomic positions were refined as distortion modes of a parent $Pm\bar{3}m$ phase as given by the ISODISTORT suite (Campbell *et al.*, 2006). The *Pnma* supercell is related to its parent by the transformation matrix [[1 0 1], [0 2 0], [−1 0 1]], with its origin at (0, 0, 0). This structural transformation replaces the seven independent atomic position parameters of the *Pnma* space-group with seven distortion modes corresponding to two A-site cation displacements [R_5^+ (A) and X_5^+ (A)], two octahedral tilt/rotations about the *b*- and *a*-axes [M_3^+ (O) and R_4^+ (O)], and three octahedral distortions [M_2^+ (O), R_5^+ (O), and X_5^+ (O)], where X_5^+ (O) corresponds to a shear along the *a*-axis.

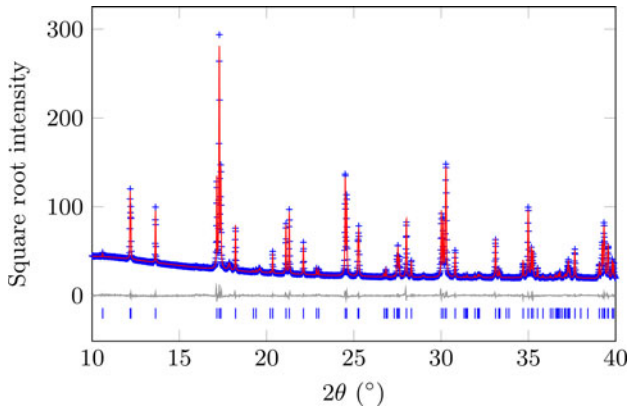

Figure 1. (Colour online) Diffraction data and Rietveld model of $SmCoO_3$ at 295 K. Data were collected over the range 3–83°2θ.

The diffraction pattern and resultant Rietveld model for the data at 295 K are shown in Figure 1, with the refined structure shown in Figure 2. A summary of the structural parameters is given in Table I, showing that this material is isostructural with $GdFeO_3$ (Geller, 1956). The supplemental information contains tables all of the structural data and the values in Figures 3–7. To account for the contribution of the impurity phase, it was modelled as a set of peaks constrained by cubic $P\bar{4}3n$ symmetry, with changes in peak positions, intensity, and width with changes in temperature accommodated by refining a cell parameter, scale factor, and crystallite size parameter. The relative peak intensities of the impurity phase were fixed from refinement of the room-temperature model.

The orthorhombic symmetry of this perovskite can be explained as a distortion from the parent cubic perovskite phase ($a_p \approx 3.76$ Å) with tilts, rotations, and shears in the CoO_6 octahedra and translations of the Sm atom (Glazer, 1975). The orthorhombic lattice parameters are given by $a \approx c \approx (\sqrt{2})a_p$ and $b \approx 2a_p$. No evidence was found for site occupancies of less than 100%, with all changes in intensity and peak position able to be described by changes in atom positions, unit-cell parameters, and isotropic displacement parameters. There was no evidence of preferred orientation.

The temperature dependence of the distortion modes, as it influenced the Sm position and CoO_6 octahedral tilt, rotation, and shear are given in Figures 3–5. The data were denoised by

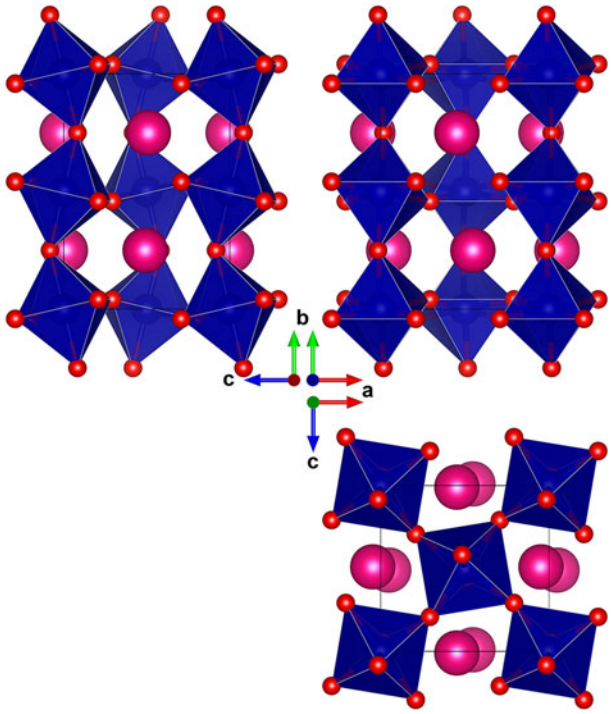

Figure 2. (Colour online) The structure of $SmCoO_3$ at 295 K. The images clearly show the tilt and rotation of the CoO_6 corner-sharing octahedra, as well as the offset of the Sm atoms from the face of the unit cell. Distortion of the octahedra is minimal.

https://doi.org/10.1017/S0885715617000872 Published online by Cambridge University Press

TABLE I. Crystal data for $SmCoO_3$ at selected temperatures. Space-group *Pnma*, $Z = 4$. Molar mass = 257:29 g mol^{-1}. By space-group symmetry, Sm y & O2 $y = ¼$, and Co x; y; $z = 0$; 0; 0. The structure data for the remaining temperatures are available in the supplemental information.

	295 K	830 K	1245 K
a (Å)	5.362 267(12)	5.459 411(10)	5.505 157(13)
b (Å)	7.510 380(14)	7.606 208(12)	7.671 64(2)
c (Å)	5.292 981(11)	5.360 822(9)	5.405 593(17)
Volume (Å^3)	213.1624(8)	222.6103(7)	228.2975(11)
Density (g cm^{-3})	8.017 22(3)	7.676 96(2)	7.485 72(4)
Sm x	0.547 48(5)	0.547 23(7)	0.545 86(6)
Sm z	−0.009 70(5)	−0.009 37(7)	−0.008 81(10)
O1 x	0.2919(5)	0.2938(5)	0.2932(6)
O1 y	0.0414(3)	0.0406(3)	0.0410(4)
O1 z	0.7919(5)	0.7938(5)	0.7932(6)
O2 x	−0.0162(1)	−0.0173(1)	−0.0135(8)
O2 z	0.0828(6)	0.0812(5)	0.0820(8)
Sm B (Å^2)	0.7119(5)	1.7016(8)	2.4282(15)
Co B (Å^2)	0.5333(13)	1.0966(18)	1.542(3)
O1 B (Å^2)	0.526(5)	1.822(5)	2.838(7)
O2 B (Å^2)	0.835(8)	1.937(9)	2.578(13)

numerical differentiation and antidifferentiation (Chartrand, 2011), with $\alpha = 0.01$ for the translations and 0.05 for the octahedral distortions. Both the A-site translational distortions, R_5^+ (A) and X_5^+ (A), were found to be significant. Only the octahedral M_3^+ (O), R_4^+ (O), and X_5^+ (O) distortions were found to be significant, with the negligible M_2^+ (O) and R_5^+ (O) distortions fixed at zero. The R_4^+ (O) distortion is a tilting of the CoO_6 octahedra about the a-direction, and the M_3^+ (O) distortion is a rotation of the octahedra about the b-direction. The X_5^+ (O) distortion is a shearing of the apical oxygen of the CoO_6 octahedra in the a-direction. The distortion magnitudes were converted to fractional coordinates and tilt/rotation/shear angles by the following formulae:

$$\text{Sm } x = \frac{1}{2} + 0.093\,99X_5^+,$$

$$\text{Sm } z = 0.093\,99R_5^+,$$

$$\text{Oct.rot.} = \arctan\left[\frac{0.066\,46R_4^+ c}{(1/4)b}\right],$$

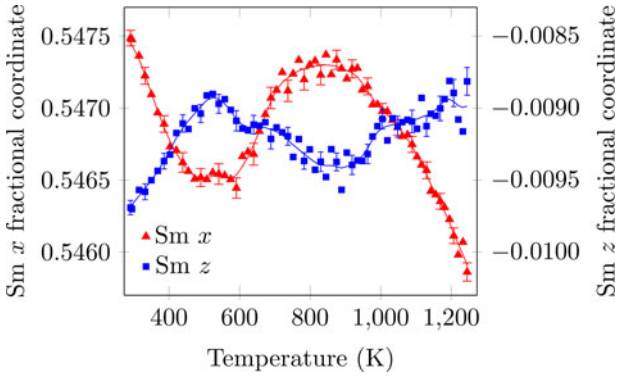

Figure 3. (Colour online) Sm fractional x- and z-coordinates as a function of temperature. The R_5^+ and X_5^+ distortions correspond to translations of the Sm atom in the z- and x-directions, respectively. The solid line is the denoised data. Error bars are given for every third data point and represent one estimated standard deviation.

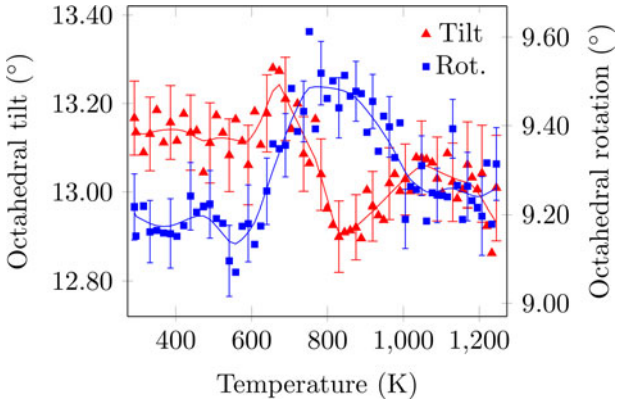

Figure 4. (Colour online) CoO_6 octahedral tilt and rotation distortion as a function of temperature. The solid line is the denoised data. Error bars are given for every third data point and represent one estimated standard deviation.

$$\text{Oct.tilt} = \arctan\left[\frac{a(-[1/4] - 0.046\,99M_3^+)}{c([1/4] - 0.046\,99M_3^+)}\right],$$

$$\text{Oct.shear} = \arctan\left[\frac{0.093\,99X_5^+ a}{(1/4)b}\right],$$

where the decimal values were given by the output of the ISODISTORT suite (Campbell *et al.*, 2006).

The A-site translational distortions are anticorrelated, with the Sm atom moving diagonally in the xz-plane with changes in temperature. The octahedral tilt and rotation also tend to occur in opposite directions; as the tilt increases, the rotation decreases. The octahedral shear appears to follow the same behaviour as the octahedral tilt, but leading those changes by about 140 K.

The temperature dependence of the unit-cell parameters is shown in Figure 6. Both the instantaneous and average linear TECs are shown in Figure 7, clearly showing both their nonlinearity and anisotropy. The instantaneous and average TECs were calculated as

$$\text{TEC}_{\text{inst.}} = \frac{1}{l}\frac{\mathrm{d}l}{\mathrm{d}T},$$

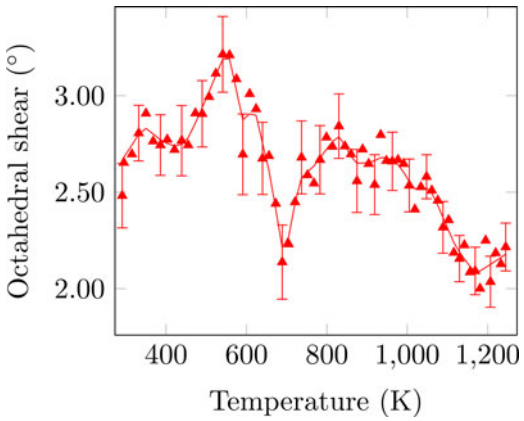

Figure 5. (Colour online) CoO_6 octahedral shear distortion as a function of temperature. The solid line is the denoised data. Error bars are given for every third data point and represent one estimated standard deviation.

https://doi.org/10.1017/S0885715617000872 Published online by Cambridge University Press

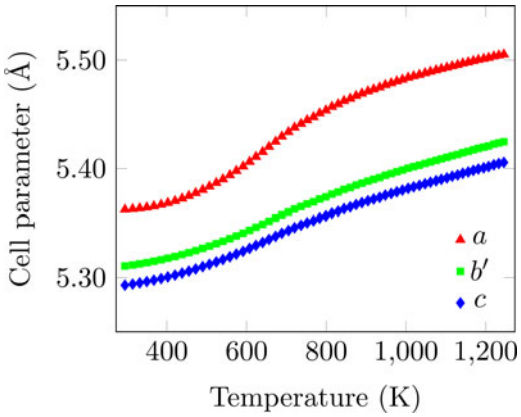

Figure 6. (Colour online) Unit-cell parameters as a function of temperature. The non-linear expansion behaviour of all three axes is clear. The error bars are smaller than the data points. $b' = b/\sqrt{2}$.

$$\mathrm{TEC}_{\mathrm{ave}} = \frac{1}{l_0}\frac{\Delta l}{\Delta T},$$

where l and l_0 are the current and initial cell parameters, respectively, and Δ represents the difference between the current value of the cell parameter or temperature and its initial value. The derivative was calculated numerically (Chartrand, 2011). The bulk TECs calculated from the data of Tu *et al.* (1997) are also given for the comparison. The maximum instantaneous and average TECs are given in Table II.

Overall, the unit cell expands much more in the *a*-direction than the *b*- and *c*-directions, where the expansion is essentially equal. The peak average TEC in the *a*-direction occurs at approximately 800 K, which is well within the operating range of intermediate-temperature solid-oxide fuel cells (Brett *et al.*, 2008), and is much greater than any of the values given by (Sun *et al.*, 2009). Above this temperature, the thermal expansion is still non-linear, but to a greatly reduced degree. Comparison of the average TECs with the bulk TECs of Tu *et al.* (1997) shows that a simple average of the TECs of the three crystallographic directions can explain the bulk measurements.

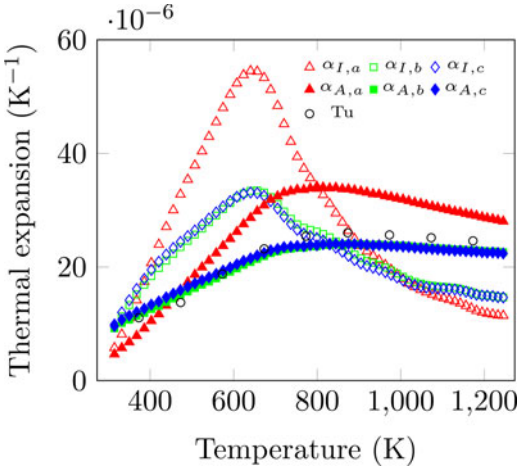

Figure 7. (Colour online) Instantaneous (I) and average (A) linear thermal expansion coefficients (TECs) for the three cell parameters showing the expansion anisotropy. The open circles are bulk TECs calculated from the results of Tu *et al.* (1997). The point of maximum orthorhombic distortion occurs at the high-temperature crossover of the instantaneous coefficients at ~1000 K.

TABLE II. Maximum instantaneous and average thermal expansion coefficients (TECs) and their respective temperatures and crystallographic direction. The uncertainties incorporate a coverage factor of 2 and the uncertainties were estimated from the magnitudes of the average uncertainties.

Axes	Instantaneous ($\times 10^{-6}$ K^{-1})	Temperature (K)	Average ($\times 10^{-6}$ K^{-1})	Temperature (K)
a	54.5(6)	640	34.0(3)	814
b	33.5(4)	656	24.05(17)	875
c	33.1(4)	640	24.10(18)	845

The large anisotropy and non-linearity in the TECs below 900 K has implications for the structural integrity of polycrystalline monoliths and for joints between different solid-oxide fuel cell components, as repeated temperature cycling may induce cracking and delamination. The point of greatest orthorhombic distortion occurs at ~1000 K, where the instantaneous TECs crossover. The maximum of the instantaneous TEC for all three axes occurs at ~640 K, showing that the gross relative changes in the average TEC for all three axes are the same.

IV. CONCLUSIONS

The crystal structure and thermal expansion of the perovskite $SmCoO_3$ have been determined over the temperature range 295–1245 K. The structure was found to be orthorhombic (*Pnma*) and isostructural with $GdFeO_3$ over the entire temperature range. The thermal expansion is both non-linear and anisotropic with a maximum average linear TEC of $34.0(3) \times 10^{-6}$, $24.05(17) \times 10^{-6}$, and $24.10(18) \times 10^{-6}$ K^{-1} along the *a*-, *b*-, and *c*-axes, respectively, between 814 and 875 K. Structural information is available in the supplemental information and select temperatures have been uploaded to the Crystallography Online Database.

SUPPLEMENTARY MATERIAL

The supplementary material for this article can be found at https://doi.org/10.1017/S0885715617000872.

ACKNOWLEDGEMENTS

This research was undertaken on the Powder Diffraction beamline at the Australian Synchrotron, Victoria, Australia.

Brett, D. J., Atkinson, A., Brandon, N. P., and Skinner, S. J. (**2008**). "Intermediate temperature solid oxide fuel cells," Chem. Soc. Rev. **37**(8), 1568–1578.

Bruker AXS (**2014**). *Topas*. Ver. 5.

Campbell, B. J., Stokes, H. T., Tanner, D. E., and Hatch, D. M. (**2006**). "Isodisplace: a web-based tool for exploring structural Distortions," J. Appl. Crystallogr. **39**(4), 607–614.

Chartrand, R. (**2011**). "Numerical differentiation of noisy, nonsmooth data," ISRN Appl. Math. **2011**, 164564.

Chen, K., Li, N., Ai, N., Cheng, Y., Rickard, W. D., and Jiang, S. P. (**2016**). "Polarization-induced interface and Sr segregation of *in situ* assembled $La_{0.6}Sr_{0.4}Co_{0.2}Fe_{0.8}O_{3-\delta}$ electrodes on Y_2O_3–ZrO_2 electrolyte of solid oxide fuel cells," ACS Appl. Mater. Interfaces **8**(46), 31729–31737.

Coelho, A. A. (**2003**). "Indexing of powder diffraction patterns by iterative use of singular value decomposition," J. Appl. Crystallogr. **36**(1), 86–95.

Dong, F., Chen, D., Ran, R., Park, H., Kwak, C., and Shao, Z. (**2012**). "A comparative study of $Sm_{0.5}Sr_{0.5}MO_{3-\delta}$ (M = Co and Mn) as oxygen

reduction electrodes for solid oxide fuel cells," Int. J. Hydrog. Energy **37** (5), 4377–4387.

Fukunaga, H., Koyama, M., Takahashi, N., Wen, C., and Yamada, K. (**2000**). "Reaction model of dense $Sm_{0.5}Sr_{0.5}CoO_3$ as SOFC cathode," Solid State Ion. **132**(3–4), 279–285.

Geller, S. (**1956**). "Crystal structure of gadolinium orthoferrite, $GdFeO_3$," J. Chem. Phys. **24**(6), 1236.

Glazer, A. M. (**1975**). "Simple ways of determining perovskite structures," Acta Crystallogr. A **31**(6), 756–762.

Hahn, T. (ed.) (**1995**). *International Tables for Crystallography* (Kluwer Academic Publishers, Dordrecht, The Netherlands), 4th ed.

Ishihara, T., Honda, M., Shibayama, T., Minami, H., Nishiguchi, H., and Takita, Y. (**1998**). "Intermediate temperature solid oxide fuel cells using a new $LaGaO_3$ based oxide ion conductor," J. Electrochem. Soc. **145**(9), 3177.

Kharko, O. V., Vasylechko, L. O., Ubizskii, S. B., Pashuk, A., and Prots, Y. (**2014**). "Structural behaviour of continuous solid solution $SmCo_{1-x}Fe_xO_3$," Funct. Mater. **21**(2), 226–232.

Pérez-Cacho, J., Blasco, J., García, J., and Sanchez, R. (**2000**). "Relationships between structure and physical properties in $SmNi_{1-x}Co_xO_3$," J. Solid State Chem. **150**(1), 145–153.

Rietveld, H. M. (**1969**). "A profile refinement method for nuclear and magnetic structures," J. Appl. Crystallogr. **2**(2), 65–71.

Rowles, M. R. (**2012**). "CONVAS2: a program for the merging of diffraction data," Powder Diffr. **25**(3), 297–301.

Sabine, T. M., Hunter, B. A., Sabine, W. R., and Ball, C. J. (**1998**). "Analytical expressions for the transmission factor and peak shift in absorbing cylindrical specimens," J. Appl. Crystallogr. **31**(1), 47–51.

Scarlett, N. V. Y., Rowles, M. R., Wallwork, K. S., and Madsen, I. C. (**2011**). "Sample-displacement correction for whole-pattern profile fitting of powder diffraction data collected in capillary geometry," J. Appl. Crystallogr. **44**(1), 60–64.

Schmitt, B., Brönnimann, C., Eikenberry, E. F., Gozzo, F., Hörmann, C., Horisberger, R., and Patterson, B. (**2003**). "Mythen detector system," Nucl. Instrum. Methods Phys. Res. A **501**(1), 267–272.

Shao, Z., Zhou, W., and Zhu, Z. (**2012**). "Advanced synthesis of materials for intermediate-temperature solid oxide fuel cells," Prog. Mater. Sci. **57**(4), 804–874.

Stinton, G. W. and Evans, J. S. (**2007**). "Parametric rietveld refinement," J. Appl. Crystallogr. **40**(1), 87–95.

Sun, C., Hui, R., and Roller, J. (**2009**). "Cathode materials for solid oxide fuel cells: a review," J. Solid State Electrochem. **14**(7), 1125–1144.

Taylor, D. (**1984**). "Thermal expansion data: III. Sesquioxides, M_2O_3, with the corundum and the a-, B- and C-M_2O_3 structures," Br. Ceram. Trans. J. **83**(4), 92–98.

Tu, H., Takeda, Y., Imanishi, N., and Yamamoto, O. (**1997**). "$Ln_{1-x}Sr_xCoO_3$ (Ln = Sm, Dy) for the electrode of solid oxide fuel cells," Solid State Ionics **100**(3–4), 283–288.

Wallwork, K. S., Kennedy, B. J., and Wang, D. (**2007**). "The high resolution powder diffraction beamline for the australian synchrotron," AIP Conf. Proc. **879**, 879–882.

Wang, J. X., Tao, Y. K., Shao, J., and Wang, W. G. (**2009**). "Synthesis and properties of $(La_{0.75}Sr_{0.25})_{0.95}MnO_{3\pm\delta}$ nano-powder prepared via Pechini route," J. Power Sources **186**(2), 344–348.

Xia, C., Rauch, W., Chen, F., and Liu, M. (**2002**). "$Sm_{0.5}Sr_{0.5}CoO_3$ cathodes for low-temperature SOFCs," Solid State Ion. **149**(1–2), 11–19.

Yang, L., Zuo, C., Wang, S., Cheng, Z., and Liu, M. (**2008**). "A novel composite cathode for low-temperature SOFCs based on oxide proton conductors," Adv. Mater. **20**(17), 3280–3283.

https://doi.org/10.1017/S0885715617000872 Published online by Cambridge University Press